

Tsai-Wu based Orthotropic Damage Model

M.R.T. Arruda^a, L. Almeida-Fernandes^b, L. Castro^c, and J.R. Correia^d

^a Research Associate, CERIS, Instituto Superior Técnico, Universidade de Lisboa, Portugal

(mario.rui.arruda@tecnico.ulisboa.pt)

^b PhD Student, CERIS, Instituto Superior Técnico, Universidade de Lisboa, Portugal

(lourenco.a.fernandes@tecnico.ulisboa.pt)

^c Associate Professor, CERIS, Instituto Superior Técnico, Universidade de Lisboa, Portugal

(luis.santos.castro@tecnico.ulisboa.pt)

^d Full Professor, CERIS, Instituto Superior Técnico, Universidade de Lisboa, Portugal

(joao.ramoa.correia@tecnico.ulisboa.pt)

Abstract: This paper presents a novel approach concerning the development of an orthotropic damage model for composite materials, based on the original plane stress Tsai-Wu failure criterion. In its original formulation, the Tsai-Wu is a mode-independent criterion only capable of acknowledging the existence of damage in a certain point of a composite material. It is not capable of identifying if the damage is located in the fibre, matrix or interlaminar zone. This study aims at filling this gap in knowledge by providing a simple method, based on equivalent stresses and strains, that identifies the relevant failure modes when the Tsai-Wu failure criterion is at the onset of damage. Using this novel methodology, it is possible to implement classical damage evolution constitutive laws based on the fracture energy regularization. At present, the proposed damage formulation is based on the consideration of a plane stress space and Mode I fracture, but its generalization to a full 3D damage model is expected to be defined in the near future. The damage model is implemented in the commercial finite element software ABAQUS through a user-defined material (UMAT) subroutine, and all numerical models are compared with experimental results available in the literature.

Keywords: Tsai-Wu Criterion, Orthotropic Damage Model, Energy Regularization, Plane Stress Formulation.

1 Introduction

Presently, several orthotropic damage models for composite materials are available in the literature, with different failure criteria and damage evolution constitutive laws [1]. Some are applied directly to the laminate, while others refer to the individual layers (plies) of the laminate [2], and all of them entail different post-failure behaviour beyond first ply failure [3].

One of the main drawbacks of most orthotropic damage models is that they present a mode dependent failure criterion, which leads to some convergence issues in terms of non-linear analysis. Moreover, since most of them are not written in terms of invariant quantities, they are axis dependent. Some authors have corrected this last problem, by using invariant base methods in the mode dependent failure [4]. The importance of an invariant orthotropic damage model, is that there is no dependency to the principal material direction, when assigning a global axis.

This is significant when variations in the stress field occur outside the materials principal direction, which has been the case for some recent composite structures produced in 3D printers [5].

The Tsai-Wu failure criterion is based on the original formulation of Gol'denblat-Kopnov [6], which is based on a general strength theory, using tensor polynomial stress space based invariants. This criterion is not as popular as the Hashin family based criteria [7], due to a difficulty associated with the computation of strength terms in biaxial test conditions [8], and the computation of fracture modes [9]. This criterion uses a quadratic failure function, which in its original formulation is a closed surface; however, in the work of [10] it was recently demonstrated that this is not necessary in order to use the criterion for different types of materials.

In this work, we propose the use of the Tsai-Wu 2D failure surface to assemble a new orthotropic damage model, in which it is possible to distinguish between fibre, matrix and shear damage, just like in the Hashin family mode dependent damage models. This new constitutive relation is implemented in the commercial finite element software ABAQUS standard, by means of user-defined material (UMAT) subroutines with Fortran.

1.1 Research Significance and Objectives

According to the authors' best knowledge, no orthotropic damage model based on Tsai-Wu failure criterion is available for homogenized composites, in which dependent failure modes are still achievable through the use of new state variables. This work plans to fill this gap in knowledge.

This model is based on a physically non-linear analysis of a homogenized GFRP laminate, which is commonly used in civil engineering structural solutions. This type of analysis is computationally more effective than the ply discount method [1], which is more popular in classical orthotropic damage models.

2 Orthotropic Damage Model

This section describes first the Tsai-Wu failure criterion, both in terms of concept and thermodynamic validation for orthotropic materials. Next, the damage evolution constitutive laws are presented, for fibre and matrix failure, by using new state variables and equivalent stresses and strains, all of which are thermodynamically admissible. The model is regularized using classical fracture energy and viscous regularization. The damage model based on Hashin failure criteria is also used, but its description is fully presented in the work of Almeida et al. [11, 12].

2.1 Constitutive Relation

For a plane stress space formulation, the constitutive relation of damaged orthotropic materials is based on a 4th order secant stiffness tensor. The relation between the independent

components of the stress and strain tensors may be expressed in the matrix form presented in equation (1).

$$\begin{Bmatrix} \sigma_1 \\ \sigma_2 \\ \tau_{12} \end{Bmatrix} = \frac{1}{D} \begin{bmatrix} (1-d_f)E_1 & (1-d_f)(1-d_m)\nu_{21}E_2 & 0 \\ (1-d_f)(1-d_m)\nu_{12}E_1 & (1-d_m)E_2 & 0 \\ 0 & 0 & (1-d_s)GD \end{bmatrix} \begin{Bmatrix} \varepsilon_1 \\ \varepsilon_2 \\ \gamma_{12} \end{Bmatrix} \quad (1)$$

with $D = 1 - (1-d_f)(1-d_m)\nu_{12}\nu_{21}$

$$\begin{Bmatrix} \hat{\sigma}_1 \\ \hat{\sigma}_2 \\ \hat{\tau}_{12} \end{Bmatrix} = \begin{Bmatrix} \sigma_1/(1-d_f) \\ \sigma_2/(1-d_m) \\ \tau_{12}/(1-d_s) \end{Bmatrix} = \frac{1}{D} \begin{bmatrix} E_1 & (1-d_m)\nu_{21}E_2 & 0 \\ (1-d_f)\nu_{12}E_1 & E_2 & 0 \\ 0 & 0 & GD \end{bmatrix} \begin{Bmatrix} \varepsilon_1 \\ \varepsilon_2 \\ \gamma_{12} \end{Bmatrix} \quad (2)$$

The damage variables d_f, d_m, d_s , corresponding to the fibre, matrix and shear failure modes, are fully described in section 2.4. A particular aspect of this composite damage model is that the shear damage is indirectly computed using information obtained for the fibre and matrix damage. It is important to point out that the shear damage evolution based on the tensile/compressive fibre and matrix damage is only an assumption, without any valid mathematical proof.

These damage variables are written in terms of tension behaviour (d_{ft}, d_{mt}) and compression behaviour (d_{fc}, d_{mc}), in the fibre and matrix directions, which are assumed to be principal material directions. Once the material is damaged, the elastic secant constitutive relation is written as defined by equation (1), in which E_1 is the elastic modulus in the fibre direction, E_2 is the elastic modulus in the matrix direction, G is the in-plane shear modulus, ν_{12} and ν_{21} are the Poisson coefficients in the fibre and matrix directions, respectively.

The definition of effective stresses is based on theoretical orthotropic damage mechanics that verify all of the tensor stress equilibrium conditions [13]. The effective stress $\hat{\sigma}$ is computed using the linear transformation presented in equation (2).

2.2 Tsai-Wu Failure Criterion

The Tsai-Wu theory is based on a classical stress tensor polynomial failure criterion for the general strength of anisotropic materials, as generically defined by equation (3). In this work, in order to verify the increase of the Tsai-Wu index (3) associated to the increase of strains, the effective stresses, defined by equation (2), are used.

$$F_1\hat{\sigma}_1 + F_2\hat{\sigma}_2 + 2F_{11}\hat{\sigma}_1\hat{\sigma}_2 + F_{11}\hat{\sigma}_1^2 + F_{22}\hat{\sigma}_2^2 + F_{66}\hat{\tau}_{12}^2 = TW(\hat{\sigma}_i, F_{jk}) \leq 1.0 \quad (3)$$

$$F_{TW} = TW(\hat{\sigma}_i, F_{jk}) - 1 = 0 \quad (4)$$

$$F_{11} = \frac{1}{X_t X_c} \quad F_{22} = \frac{1}{Y_t Y_c} \quad F_1 = \frac{1}{X_t} - \frac{1}{X_c} \quad F_2 = \frac{1}{Y_t} - \frac{1}{Y_c} \quad F_{66} = \frac{1}{S_L S_T} \quad (5)$$

$$F_{12} = \frac{1}{2B_{t,xy}^2} \left(1 - B_{t,xy}(F_1 + F_2) - B_{t,xy}^2(F_{11} + F_{22}) \right) \leq \sqrt{F_{11}F_{22}} \quad (6)$$

$$F_{12} = -\frac{1}{2}\sqrt{F_{11}F_{22}} \quad (7)$$

In equations (3) and (4), the terms F_i and F_{ii} , defined by equation (5), are second order strength tensors, and are related to the one directional engineering strengths, which are easily measured in laboratory. The interaction term F_{12} is provided from biaxial test conditions, and according to some early theories, these must be selected with caution to obtain accurate values for the strength tensors [14]. These terms must obey to the inequality defined in equation (6) to ensure a definition of a closed surface for which it is possible to demonstrate that for isotropic materials, if F_{12} obeys to equation (7), the classical Von-Mises criterion is recovered. The material parameters depend on the stress direction and sign: X_t and Y_t are the tension limit strength of the fibre and matrix, respectively; X_c and Y_c are the compression limit strength of the fibre and matrix, respectively; S_L corresponds to the longitudinal shear resistance; S_T is the transverse shear resistance.

It is known that some composites do not satisfy condition (6), as referred in the work of [10]. Recently it was mathematically demonstrated that this condition can be relaxed under some circumstances [10]. In any case, for the range of composites used in this work, the term F_{12} still verifies inequality (6).

$$B_{t,xy} = \min \left\{ \frac{Y_t}{1 - \nu_{21}}; \frac{X_t}{1 - \nu_{12}} \right\} \quad (8)$$

The main difficulty is to obtain the term $B_{t,xy}$, which is the tensile bi-stress strength. This term can be estimated using the several outputs from the World-Wide Failure Exercise [15], in which it is possible to obtain a lower-bound estimate using the maximum failure envelope, as written in equation (8). In any case, several authors have proven that the exact value of F_{12} is almost irrelevant for normal engineering applications [16, 17], as it only tilts the failure ellipse of the Tsai-Wu function.

2.3 Thermodynamic Admissibility

All continuum damage models require the definition of an evolution law, and must be consistent with the first and second thermodynamic laws [1, 18].

$$\Psi = \Psi(\sigma, d_i, z_j) \quad (9)$$

To use these constitutive laws it is necessary to define a thermodynamic potential function, denoted here as Ψ (9). The variables d_i and z_j are used to control the dissipation mechanism of the material, which is not measurable, and are usually defined as internal state variables. The variable z_j (defined below), is used to control the spread of damage, in certain directions, when effective stresses are not predominant. This is necessary to control the fibre and matrix damage distribution, since the Tsai-Wu criterion is only one general inequality.

$$\begin{cases} \varepsilon = \frac{\partial \Psi}{\partial \sigma} \\ Y_i = \frac{\partial \Psi}{\partial d_i} \\ Z_j = \frac{\partial \Psi}{\partial z_j} \end{cases} \quad (10)$$

$$Y_i \delta d_i \geq 0 \quad \& \quad Z_j \delta z_j \geq 0 \quad (11)$$

It is possible to define a set of associated variables by deriving the potential Ψ . Conventionally, Y are referred in the scientific community as the thermodynamic forces. It is beyond the scope of this work, but it can be demonstrated that a damage model is thermodynamically admissible [19] if the thermodynamic forces, defined in (10), fulfil the equations (11) [1, 18].

$$F_{TW}(\sigma, d, z) \leq 0 \quad (12)$$

To assemble a damage model, it is necessary to define a “loading function” that may depend on the primary and secondary state variables, as expressed in (12). The most common definition for this function is to use negative values for the elastic domain, and a null value when the material can dissipate energy by developing damage.

$$\begin{aligned} F_{TW} \leq 0 \quad &\& \quad \delta d \geq 0 \quad &\& \quad \delta d \cdot F_{TW} = 0 \\ &\& \quad \delta z \geq 0 \quad &\& \quad \delta z \cdot F_{TW} = 0 \end{aligned} \quad (13)$$

It can be demonstrated that when using equations (11) and (12), it is possible to formulate the known loading/unloading Kuhn-Tucker conditions [20], as expressed by equations (13). The first two inequalities define the domain of validity of each variable, *i.e.* the dissipation potential must be non-positive and the damage increments cannot be negative. The third expression relates both variables imposing that in order to have damage increments the dissipation potential must be null.

$$\begin{aligned} \Psi(\sigma, d, z) &= \frac{1}{2} \{\sigma\}^t [C_d] \{\sigma\} \\ \Psi(\sigma, d, z) &= \frac{1}{2E_1} \left(\frac{\langle \sigma_1 \rangle^2}{1 - d_{ft}^z} + \frac{\langle -\sigma_1 \rangle^2}{1 - d_{fc}^z} \right) + \frac{1}{2E_2} \left(\frac{\langle \sigma_2 \rangle^2}{1 - d_{mt}^z} + \frac{\langle -\sigma_2 \rangle^2}{1 - d_{mc}^z} \right) - \frac{\nu_{12}\sigma_1\sigma_2}{E_1} + \frac{\tau_{12}^2}{G(1 - d_s^z)} \quad (14) \end{aligned}$$

$$d_{fm,tc}^z = z_{fm,tc} d_{fm,tc}$$

where $\langle \rangle$ is the Macauley bracket operator, defined for every $\alpha \in \mathcal{R}$, $\langle \alpha \rangle = \frac{\alpha+|\alpha|}{2}$.

Since the Tsai-Wu failure criterion is written in terms of stresses, the Gibbs energy density defined in equation (14) is used. As defined by [21], two type of internal state variables are taken into account: the damage, d , and the state direction variable, z , for fibre and matrix in tension and compression. This function must be positive definite, and it must be zero at the origin with respect to the free variables.

$$\{Y\} = \frac{1}{2} \begin{Bmatrix} \frac{\langle \sigma_1 \rangle^2}{E_1(1 - d_{ft})^2} \\ \frac{\langle -\sigma_1 \rangle^2}{E_1(1 - d_{fc})^2} \\ \frac{\langle \sigma_2 \rangle^2}{E_2(1 - d_{mt})^2} \\ \frac{\langle -\sigma_2 \rangle^2}{E_2(1 - d_{mc})^2} \\ \frac{\tau_{12}^2}{G(1 - d_s)^2} \end{Bmatrix} \quad (15)$$

The thermodynamic forces are defined by equation (15), for the fibre, matrix and shear damage, in tension and compression. Since these quantities are always positive, the condition (11) is verified if the damage variable never decreases. This is important since it allows for a simplification of the model when formulating the “evolution constitutive law” [1, 22].

2.4 Orthotropic Damage Definition

$$d_f = \begin{cases} d_{ft} & \text{if } \hat{\sigma}_1 \geq 0 \\ d_{fc} & \text{if } \hat{\sigma}_1 < 0 \end{cases} \quad (16)$$

$$d_m = \begin{cases} d_{mt} & \text{if } \hat{\sigma}_2 \geq 0 \\ d_{mc} & \text{if } \hat{\sigma}_2 < 0 \end{cases} \quad (17)$$

$$d_s = 1 - (1 - d_{ft})(1 - d_{fc})(1 - d_{mt})(1 - d_{mc}) \quad (18)$$

In order to compare different orthotropic damage models, the classical damage attribution presented in equations (16) to (18) will be initially used. This is normally found in the Hashin based family composite damage models.

$$d_f = 1 - (1 - d_{ft})(1 - d_{fc}) \quad (19)$$

$$d_m = 1 - (1 - d_{mt})(1 - d_{mc}) \quad (20)$$

$$d_s = 1 - \sqrt{(1 - d_{ft})(1 - d_{fc})(1 - d_{mt})(1 - d_{mc})} \quad (21)$$

A different damage definition, in equations (19) to (21), will also be considered. The reasons for this option are two-fold. Firstly, the Tsai-Wu criterion is more severe when different damage modes are activated when compared to the classical Hashin criterion (as demonstrated in the examples presented in the following sections). Therefore, the shear damage evolution may be quadratic and more brittle than the real one. Secondly, the classical damage assignments based on Hashin failure criteria do not allow for stiffness degradation when the stress signs change

due to cyclic loads. For equations (16) to (18) the term original damage evolution (ODE) is adopted, while for equations (19) to (21) the term modified damage evolution (MDE) is used.

2.5 Equivalent Stresses and Displacements

$$\sigma_{eq}\varepsilon_{eq} = \sum \sigma_{ij}\varepsilon_{ij} \quad \text{and} \quad \varepsilon_{eq} = \sqrt{\sum \varepsilon_{ij}^2} \quad (22)$$

$$\begin{cases} \varepsilon_{eq}^{f,t} = \sqrt{(\varepsilon_1)^2 + \gamma_{12}^2} & \text{if } \hat{\sigma}_1 \geq 0 \\ \varepsilon_{eq}^{f,c} = \sqrt{(-\varepsilon_1)^2 + \gamma_{12}^2} & \text{if } \hat{\sigma}_1 < 0 \\ \varepsilon_{eq}^{m,t} = \sqrt{(\varepsilon_2)^2 + \gamma_{21}^2} & \text{if } \hat{\sigma}_2 \geq 0 \\ \varepsilon_{eq}^{m,c} = \sqrt{(-\varepsilon_2)^2 + \gamma_{21}^2} & \text{if } \hat{\sigma}_2 < 0 \end{cases} \quad (23)$$

$$\begin{cases} \sigma_{eq}^{f,t} = \frac{\langle \sigma_1 \rangle \langle \varepsilon_1 \rangle + |\tau_{12}\gamma_{12}|}{\varepsilon_{eq}^{f,t}} & \text{if } \hat{\sigma}_1 \geq 0 \\ \sigma_{eq}^{f,c} = \frac{\langle -\sigma_1 \rangle \langle -\varepsilon_1 \rangle + |\tau_{12}\gamma_{12}|}{\varepsilon_{eq}^{f,c}} & \text{if } \hat{\sigma}_1 < 0 \\ \sigma_{eq}^{m,t} = \frac{\langle \sigma_2 \rangle \langle \varepsilon_2 \rangle + |\tau_{21}\gamma_{21}|}{\varepsilon_{eq}^{m,t}} & \text{if } \hat{\sigma}_2 \geq 0 \\ \sigma_{eq}^{m,c} = \frac{\langle -\sigma_2 \rangle \langle -\varepsilon_2 \rangle + |\tau_{21}\gamma_{21}|}{\varepsilon_{eq}^{m,c}} & \text{if } \hat{\sigma}_2 < 0 \end{cases} \quad (24)$$

To define the damage evolution constitutive law, new variables are created based on the definition of equivalent stresses and strains, which are computed using the general equivalent principal virtual work [23], written in the format defined by equation (22). For the particular cases of fibre and matrix directions, these equations are rewritten into equivalent strains (23) and equivalent stresses (24), both for tensile and compressive behaviours.

To minimize mesh dependency due to material softening, the constitutive law is written as a stress-equivalent displacement function, by computing a characteristic length L_c , which is directly provided by ABAQUS [24]. The equivalent displacements, given by equation (32), do not depend on the crack direction and are defined in the initial work of [25].

2.5.1 Onset of Damage Initiation

$$\begin{cases} \varepsilon_{eq,ft}^0 = \sqrt{\langle \varepsilon_1(d_{0,ft}) \rangle^2 + \gamma_{12}^2(d_{0,ft})} \\ \varepsilon_{eq,fc}^0 = \sqrt{\langle -\varepsilon_1(d_{0,fc}) \rangle^2 + \gamma_{12}^2(d_{0,fc})} \\ \varepsilon_{eq,mt}^0 = \sqrt{\langle \varepsilon_2(d_{0,mt}) \rangle^2 + \gamma_{21}^2(d_{0,mt})} \\ \varepsilon_{eq,mc}^0 = \sqrt{\langle -\varepsilon_2(d_{0,mc}) \rangle^2 + \gamma_{21}^2(d_{0,mc})} \end{cases} \quad (25)$$

$$\begin{cases} \sigma_{eq,ft}^0 = \frac{\langle \sigma_1(d_{0,ft}) \rangle \langle \varepsilon_1(d_{0,ft}) \rangle + \tau_{12}(d_{0,ft}) \gamma_{12}(d_{0,ft})}{\varepsilon_{eq,ft}^0} \\ \sigma_{eq,fc}^0 = \frac{\langle -\sigma_1(d_{0,fc}) \rangle \langle -\varepsilon_1(d_{0,fc}) \rangle + \tau_{12}(d_{0,fc}) \gamma_{12}(d_{0,fc})}{\varepsilon_{eq,fc}^0} \\ \sigma_{eq,mt}^0 = \frac{\langle \sigma_2(d_{0,mt}) \rangle \langle \varepsilon_2(d_{0,mt}) \rangle + \tau_{21}(d_{0,mt}) \gamma_{21}(d_{0,mt})}{\varepsilon_{eq,mt}^0} \\ \sigma_{eq,mc}^0 = \frac{\langle -\sigma_2(d_{0,mc}) \rangle \langle -\varepsilon_2(d_{0,mc}) \rangle + \tau_{21}(d_{0,mc}) \gamma_{21}(d_{0,mc})}{\varepsilon_{eq,mc}^0} \end{cases} \quad (26)$$

$$\hat{\sigma}_{ij} = \beta \hat{\sigma}_{ij}^{onset_of_damage} = \beta \hat{\sigma}_{ij}(d_0) \quad \Rightarrow \quad \hat{\sigma}_{ij}(d_0) \propto \varepsilon_{ij}(d_0) \quad (27)$$

$$\sigma_i(d_0) = C_{d_{ij}} \varepsilon_j(d_0) \quad (28)$$

$$\underbrace{\beta^2 (2F_{11}\hat{\sigma}_1\hat{\sigma}_2 + F_{11}\hat{\sigma}_1^2 + F_{22}\hat{\sigma}_2^2 + F_{66}\hat{\tau}_{12}^2)}_a + \underbrace{\beta (F_1\hat{\sigma}_1 + F_2\hat{\sigma}_2)}_b + \underbrace{(-1)}_c = 0 \quad (29)$$

$$\beta = \frac{-b + \sqrt{b^2 - 4ac}}{2a} \quad (30)$$

To define the damage evolution constitutive laws, it is necessary to compute the initial equivalent stresses, σ_{eq}^0 , and the initial equivalent strains, ε_{eq}^0 , defined in equations (25) and (26). It is necessary to solve the Tsai-Wu criterion for the onset of damage initiation as defined by equation (4), which corresponds to the second degree equation (29). After this, it is possible to compute the stress and strain fields on the onset of damage, and its equivalent quantities, defined in equations (27). After calculating the strain field at the onset of damage, it is possible to use the constitutive relation law (1), to compute the given stress field to be used in the equivalent stress (26).

$$\begin{cases} F_{TW}(\hat{\sigma}_1 \geq 0, \hat{\sigma}_2 = 0, \hat{\tau}_{12},) = 0 \Rightarrow \beta_{ft} \\ F_{TW}(\hat{\sigma}_1 < 0, \hat{\sigma}_2 = 0, \hat{\tau}_{12},) = 0 \Rightarrow \beta_{fc} \\ F_{TW}(\hat{\sigma}_1 = 0, \hat{\sigma}_2 \geq 0, \hat{\tau}_{12},) = 0 \Rightarrow \beta_{mt} \\ F_{TW}(\hat{\sigma}_1 = 0, \hat{\sigma}_2 < 0, \hat{\tau}_{12},) = 0 \Rightarrow \beta_{mc} \end{cases} \quad (31)$$

For each of the principal material directions, fiber and matrix in tension and compression, it is necessary to separately solve the Tsai-Wu damage initiation criterion, as referred in equations (31). The choice of these stress planes is related to the general assumption that the damage evolution depends mainly on the stresses and strains belonging to the same damage variable plane. This is in accordance to many other orthotropic damage models published earlier [26].

2.5.2 Linear Damage Evolution Constitutive Law

The linear damage evolution constitutive law is written according to the information presented in **Figure 1**, in which the area $\widehat{ABC} \Rightarrow (\varepsilon_{eq}(d = 0))$ under the curve corresponds to the fracture energy, G_f . The initial values σ_{eq}^0 and δ_{eq}^0 are computed at the onset of damage, by analytically solving equation (31). In order to obey to the Kuhn-Tucker equations (13), after the beginning of each incremental process, the “evolution law” is updated to curve $\widehat{ADC} \Rightarrow (\varepsilon_{eq}(d))$. It is also possible to use this formulation considering residual stress, which may be specially required when modelling compressive stresses, in both fibre and matrix [11].

$$\delta_{ij}^{eq} = L_c \varepsilon_{ij}^{eq} \quad \text{and} \quad \delta_{eq}^u = 2G_f/\sigma_{eq} \quad (32)$$

$$d_{fm,tc} = \frac{\delta_{eq,fm,tc}^u(\delta_{eq,fm,tc} - \delta_{eq,fm,tc}^0)}{\delta_{eq,fm,tc}^0(\delta_{eq,fm,tc}^u - \delta_{eq,fm,tc}^0)} \quad \text{if} \quad \delta_{eq,fm,tc}^0 \leq \delta_{eq,fm,tc} \leq \delta_{eq,fm,tc}^u \quad (33)$$

$$\delta_{eq}^D = \delta_{eq}^u - \sigma_{eq}^i/\sigma_{eq}^0 (\delta_{eq}^u - \delta_{eq}^0) \quad (34)$$

$$d_r = 1 - \sigma_{eq}^i/\sigma_{eq}^0 \frac{\delta_{eq}^0}{\delta_{eq}} \quad (35)$$

Once the onset of damage is reached, for a linear softening evolution, it is demonstrated in [22] that the damage variables are computed according to equation (33). When residual stresses are to be taken into account, the location of point D is defined by equation (34) and the damage evolution is defined by (35). The equivalent displacements, are calculated according to (32), which is used in the work of Bazant [25].

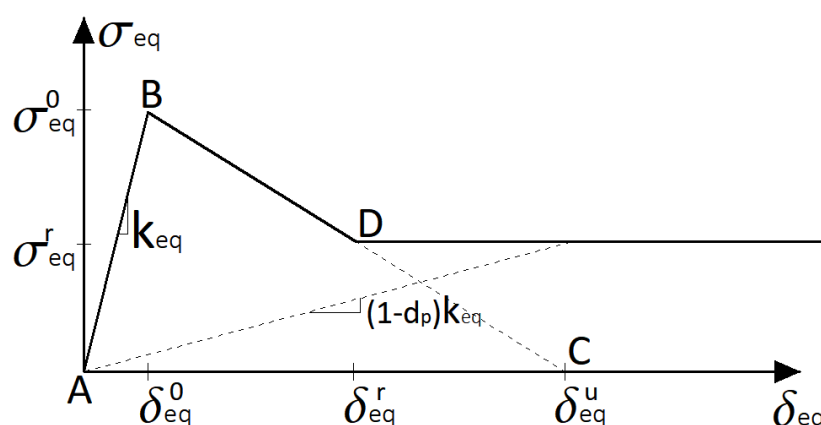


Figure 1 – Constitutive relation for linear softening.

2.5.3 Exponential Damage Evolution Constitutive Law

$$d_{fm,tc} = 1 - \frac{\delta_{eq,fm,tc}^0}{\delta_{eq,fm,tc}} \exp \left[-\frac{\sigma_{eq,fm,tc}^0}{G_{fm,tc}} (\delta_{eq,fm,tc} - \delta_{eq,fm,tc}^0) \right] \text{ if } \delta_{eq,fm,tc}^0 \leq \delta_{eq,fm,tc} \quad (36)$$

$$\delta_{eq}^D = -\frac{G_f}{\sigma_{eq}^0} \ln(\sigma_{eq}^i / \sigma_{eq}^0) + \delta_{eq}^0 \quad (37)$$

Some recent works have suggested that the exponential softening law defined in (36) is more suited to describe the tensile post-peak behaviour of pultruded GFRP materials [11, 12]. Therefore, in this work the exponential softening law will also be used in some examples, in which the tensile behaviour governs the structural response. The location of point D is given by equation (37), and equation (35) is used again to compute the residual damage evolution.

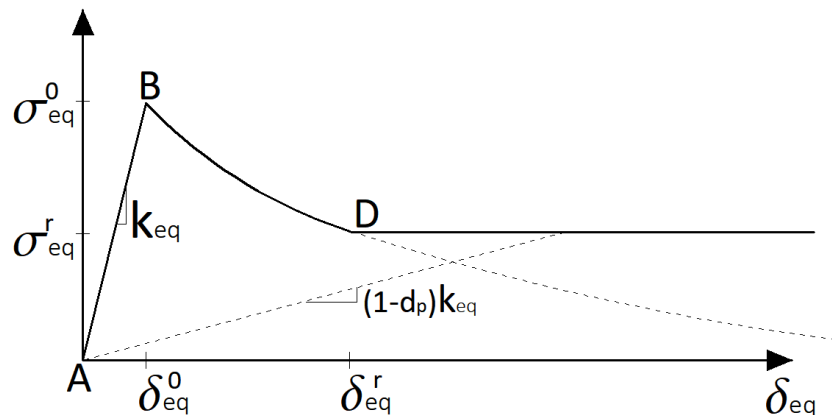


Figure 2 – Constitutive relation for exponential softening.

2.6 State Direction Variable

$$z_{ft} = \frac{\langle \hat{\sigma}_1 \rangle}{X_t} + \frac{|\hat{\tau}_{12}|}{\sqrt{S_L S_T}} \quad z_{fc} = \frac{\langle -\hat{\sigma}_1 \rangle}{X_c} + \frac{|\hat{\tau}_{12}|}{\sqrt{S_L S_T}} \quad (38)$$

$$z_{mt} = \frac{\langle \hat{\sigma}_2 \rangle}{Y_t} + \frac{|\hat{\tau}_{12}|}{\sqrt{S_L S_T}} \quad z_{mc} = \frac{\langle -\hat{\sigma}_2 \rangle}{Y_c} + \frac{|\hat{\tau}_{12}|}{\sqrt{S_L S_T}} \quad (39)$$

The state direction variable z is defined for the fibre and matrix tension and compression behaviour by equations (38) and (39), respectively. This state direction variable is necessary in order to guarantee that when the Tsai-Wu criterion is reached, not all damage modes are activated at the same time. This state variable also guarantees that in the presence of an uniaxial stress state, only one damage mode is activated, preserving the thermodynamics of the problem, something other damage models are not capable of. The effective stresses are used in

order to guarantee that the state variable always increases. As mentioned, equivalent strains were not chosen in order to prevent multi damage modes in uniaxial stress.

$$d_{fm,tc}^z = z_{fm,tc} d_{fm,tc} \quad (40)$$

$$0 \leq z_{fm,tc} \leq 1 \quad \delta z_{fm,tc} \geq 0 \quad \delta d_{fm,tc}^z (z_{fm,tc} > 0) \geq 0 \quad (41)$$

The damage variable computed using equation (40) is then corrected using equation (41), where the state direction variable is used in order to prevent the damage growth in a certain plane-axis in which the stress is not that prevalent. In any case, in the presence of biaxial stress states, the damage variables evolve just like in other damage models. In order to promote the thermodynamic admissibility of the damage model, the state variable must verify the conditions (13), that are now rewritten in equation (41) for the fibre and matrix tension and compression behaviours.

2.7 Viscous Regularization

When using only the energy regularization described in section 2.5, some issues still remain that may cause: (i) loss of positive definiteness; (ii) some localization of damage; and (iii) some numerical convergence difficulties. To overcome these problems, an efficient/simple procedure corresponds to the implementation of a viscous regularization.

When the stiffness tensor is not positive definite, damage localizes in a narrow band, and the numerical solution depends upon the numerical discretization: decreasing the element size in the localized zone the computed dissipated energy also decreases. Therefore, the structural response is not objective because it does not converge to a unique solution with mesh refinement. Moreover, when the stiffness is not positive definite, standard Newton-Rapshon techniques present convergence difficulties [27].

$$\delta d_{fm}^v = \frac{1}{\eta} (d_{fm} - d_{fm}^v) \times \delta t \quad (42)$$

As referred above, it is possible to overcome some of these drawbacks by using the viscous regularization scheme. This technique is based on an artificial Duvaut-Lions viscosity model [28]. More details on the theoretical background of this method can be found in the work of [29]. This algorithm causes the stiffness matrix of the softening material to be positive definite for sufficiently small time increments, improving convergence. In this regularization scheme, a viscous damage variable is defined by the evolution equation (42). d_{fm} is the fibre/matrix damage variable obtained as described previously, d_{fm}^v is the regularized viscous fibre/matrix damage variable, and η is the viscosity stabilization factor. The damage response of the viscous material is given by:

$$\{\sigma\} = [C_d^v]\{\varepsilon\} \quad (43)$$

where the damaged elasticity matrix, C_d^v , is computed using viscous values for the damage variables associated to each failure mode. The use of a viscous regularization with a small value assumed for the viscosity parameter (small compared to the characteristic time increment) usually helps improving the rate of convergence of the model in the softening regime, without compromising the quality of the numerical solution. The basic idea is that the solution of the viscous system relaxes to that of the inviscid case as $t/\eta \rightarrow 0$, where t represents time.

$$d_{fm}^v(t_0 + \Delta t) = \frac{\Delta t}{\eta + \Delta t} d_{fm}(t_0 + \Delta t) + \frac{\eta}{\eta + \Delta t} d_{fm}^v(t_0) \quad (44)$$

A numerical algorithm needs to be implemented for the time integration of the internal variables. Using a backward-Euler scheme [30], the internal variables can be updated, resulting in the incremental viscous damage updated variable, defined by equation (44). In this work, since the numerical problem is only 2D, the secant method is used in the iterative process at the structural level.

2.8 Implementation of the Damage Model in Abaqus

In order to allow a better understanding of the material behaviour described above, **Figure 3** presents a classical flowchart with the key steps of the UMAT implemented in ABAQUS standard. The figure shows how the damaged stress and Jacobian are calculated when the damage variable is updated. The basic steps of the UMAT are: 1st update the strain field ε_i using the iterative strain increment $\Delta\varepsilon_i$; 2nd update the total effective stress field $\hat{\sigma}_j$, using the updated strain field ε_i ; if the Tsai-Wu failure criteria is reached F_{TW} , in that integration Gauss point solve the second degree equation, in order to obtain equivalent stress and strain parameters β_k at the onset of damage; 3rd update the internal state variable damage d_{fm} and state directional variable z_{fm} ; 4th calculate the corrected directional damage d_{fm}^z ; 5th update the viscous damage d_{fm}^v ; 6th update the damaged stress $\sigma_i(d_{fm}^v)$ and Jacobian field J_{ji} .

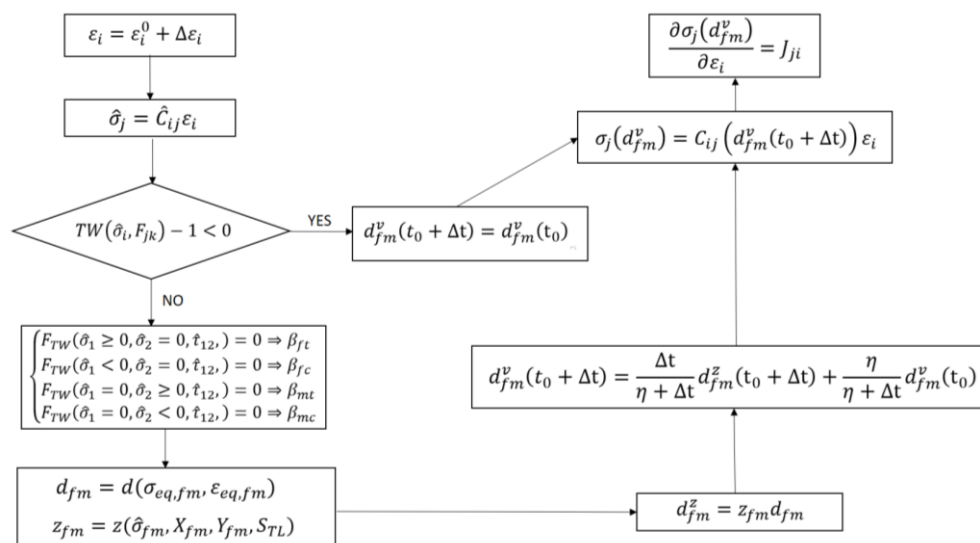


Figure 3 – Flow chart for the Tsai-Wu failure damage base model.

3 Model Verification

In order to directly compare both ODE and MDE Tsai-Wu failure based damage models, a simple 1 dof example is performed in a unit size square element **Figure 4**, with pure shear stress applied in all four sides, and consequently auto-equilibrated. This stress state will activate both fibre and matrix tensile damage, which will eventually produce different levels of shear damage, and consequently shear behaviour.

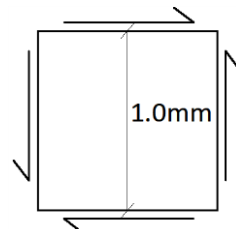
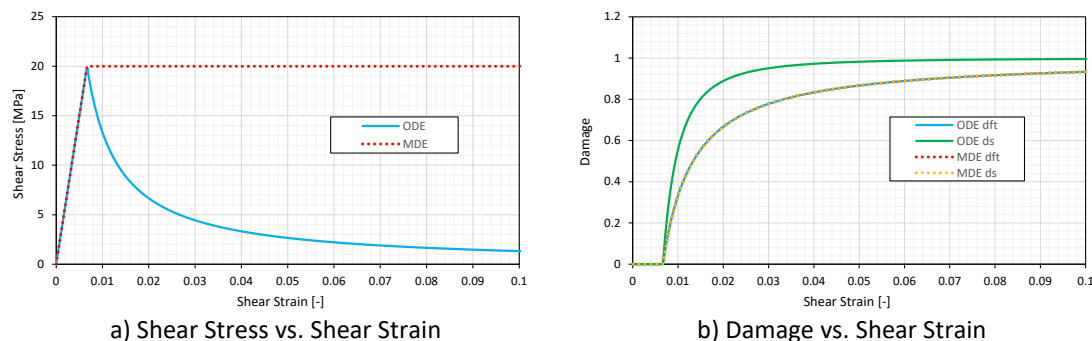


Figure 4 – Shear load application, on a unit size square element.

The adopted elastic and strength properties are respectively: $E_1 = 23GPa$, $E_2 = 12GPa$, $G = 3GPa$ and $X_t = X_c = 300MPa$; $Y_t = Y_c = 80MPa$; $S_T = S_L = 20MPa$. In order to understand the importance of the MDE proposal, it is admitted that both models are “perfectly plastic” ($G_{ft,mt} = +\infty$), for the fibre and matrix tensile damage. This is a theoretical assumption, which aims at providing a better understanding of the damage evolution.



a) Shear Stress vs. Shear Strain

b) Damage vs. Shear Strain

Figure 5 – Stress, strain and damage field on a square finite element.

In **Figure 5 a)** it is possible to observe the main differences in the shear behaviour simulated by the ODE and MDE models. Although the fibre and matrix damage evolution is “perfectly plastic” in the ODE model, it exhibits a softening regime, when the shear stress vs. shear strain curve is drawn. This is expected, since the shear damage evolution is always quadratic, with simultaneous influence of the fibre and matrix damage. This is somehow counterintuitive, since shear fracture possesses more fracture energy than fibre tensile damage. This is even more evident in **Figure 5 b)**, in which it is possible to observe that the shear damage evolution (ds) is more brittle than the fibre tensile damage (dft).

On the other hand, regarding the MDE model, when observing the shear stress vs. shear strain curve (**Figure 5 a)**), it can be seen that it preserves at least the same “perfectly plastic” behaviour during the tensile damage evolution. This is also displayed in **Figure 5 b)**, in which the fibre tensile and shear damage evolution is identical.

4 Numerical Examples

In this section three numerical examples are studied using the proposed Tsai-Wu failure model, and the modified damage model based on Hashin failure criteria applied in [11, 12]. Both damage models were implemented in the commercial software ABAQUS using the user-subroutine material (UMAT), for an implicit standard analysis. The first example corresponds to the compact tension test in a pultruded GFRP laminate, which has been widely studied in [11, 12]; this aims at validating the damage models and the efficiency of regularization techniques used to prevent mesh dependency found in the results of [31]. The second example corresponds to a three-point bending test in a GFRP beam, in which a central notch is present in order to promote tensile damage in the matrix direction. The third and last example is a classical bolted lap joint test with shear-out failure, studied with a circular hole. In all examples 4 node plane stress elements are used (CPS4R), using a reduced numerical integration scheme, and for the second and third examples, symmetry simplifications are adopted. In all examples, ODE and MDE (see section 2.4) are used with the Tsai-Wu failure model for comparative purposes.

For the damage model based on Hashin failure criteria, the shear fibre tensile parameter α is considered to be equal to 1 for all examples. This is necessary in order to produce a comparable result with the Tsai-Wu failure model in the fibre direction.

4.1 Compact Tension Test

This first example – compact tension (CT) test of a pultruded GFRP material – has already been fully studied by [11, 12, 32], and the experimental setups and numerical simulations used in those studies are fully described in the publications by those authors.

The specimen geometry adopted in this paper is the one reported in [32]. The geometry of the pultruded GFRP specimen, whose laminate thickness is 10 mm, is depicted in **Figure 6**. This specimen geometry is relevant since it provides a localized stress concentration zone that may influence the mechanical response when softening behaviour is present in the constitutive relation.

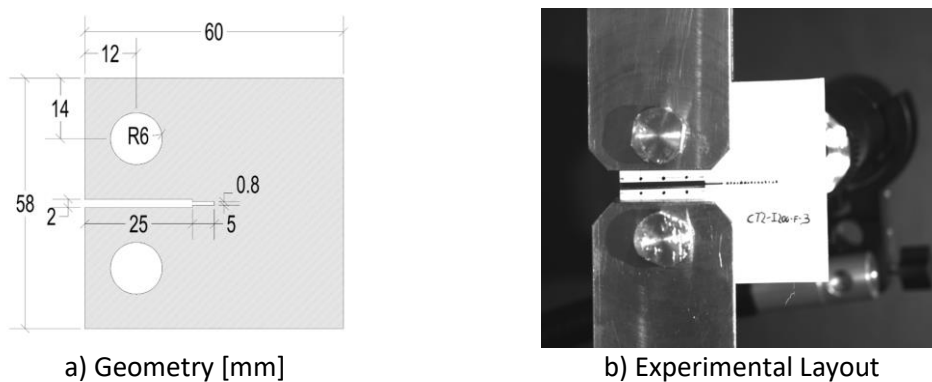


Figure 6 – Geometry and test setup for the classical compact tension test (CT).

The values for the GFRP material parameters (elastic moduli and strength) considered here (**Table 1**) are the ones detailed in the work of [32, 33]. The original work of Almeida et al. fully describes how all these properties may be obtained using standard experimental tests. The values for the failure and damage evolution parameter properties considered in the present

study are also listed in **Table 1**, for both Hashin and Tsai-Wu failure models. For the elastic material angle, it is considered that the 1-axis is the horizontal global axis (the x-axis).

Table 1 – Properties for the pultruded GFRP material used in the CT tests.

$E_1 [MPa]$	$E_2 [MPa]$	$G_{12} [MPa]$	$\nu_{12} [-]$	$X_t = X_c [MPa]$
30000	12000	3000	0.24	323
$Y_t = Y_c [MPa]$	$S_L [MPa]$	$S_T [MPa]$	$G_{ft} = G_{fc} [MPa.mm]$	$G_{mt} = G_{mc} [MPa.mm]$
71	67	64	100	20

In order to correctly simulate the nodal constraint associated to the hole where load was introduced in the experimental campaign described in [32], the vertical and horizontal displacements are restricted in half of the circle, in the top and bottom openings, as presented in **Figure 7a**). In addition, two master joints are considered, which promote a perfect kinematic tie to half of the circle, as depicted in **Figure 7 b)**. In these two master joints, the vertical off-plane and horizontal displacements are restricted, but the rotation is left free. Moreover, since the structural response presents softening, a vertical prescribed displacement is applied at the top opening (as in the experiments). Therefore, since force control is not necessary, a classical Newton-Raphson method is used to solve the non-linear governing system. The mesh is defined around the curved notch using a radial base refinement in order to guarantee a maximum element size of around 0.2 mm.

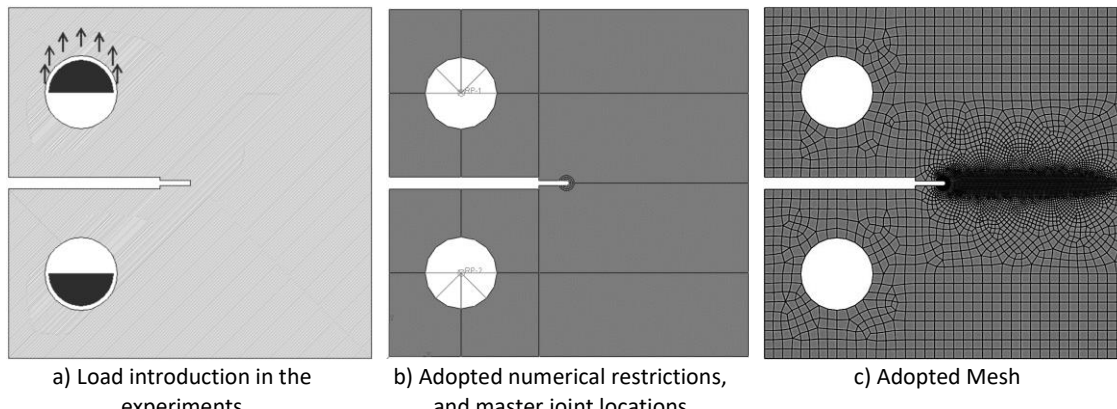


Figure 7 – Restrictions applied to the boundary conditions of the numerical model and adopted mesh.

According to the work of [32], it is possible to conclude that, for this example, both linear and exponential damage evolution in transverse tension lead to good results, namely when compared with experimental data. In the present work, for the tensile behaviour, the exponential damage evolution is used for both Hashin and Tsai-Wu failure models. However, for the compressive behaviour, linear damage evolution is adopted.

Figure 11 displays the vertical force vs. displacement in the master joint obtained in the experimental CT tests (2 specimens) and the corresponding numerical results, using Hashing and Tsai-Wu failure models, for both ODE and MDE variants. The numerical models all present a lower bound in terms of maximum load, when directly compared with the experimental results. This is an expected result as the consideration of an exponential softening law leads to a lower bound in terms of maximum reaction, as it is shown in the work of [11, 12].

It is possible to conclude that all damage models being considered lead to similar results, and in the case of the Tsai-Wu failure model, no relevant differences are noticed when using ODE or MDE variants. This was expected, since in this particular case the influence of the shear damage in the structural response is small, due to the nature of the test setup. This fact can be illustrated by observing the final shear damage distribution for both the ODE and MDE formulations in **Figure 10**. The main difference between the results provided by Hashin and Tsai-Wu failure models occurs during the softening regime. This is due to the influence of the state directional variable on the Tsai-Wu failure model.

Figure 8 and **Figure 9** show the damage evolution for the Hashin and Tsai-Wu failure models when MDE is considered. It is possible to verify that both present similar tensile fibre and matrix damage evolution. The main difference lies in the compressive fibre damage, which does not appear when the damage model based on Hashin failure is used and is very small for the Tsai-Wu failure model. This small difference of the Tsai-Wu failure model is due to the existing state direction variable, defined by equations (38) and (39), that prevents the compressive fibre damage to grow.

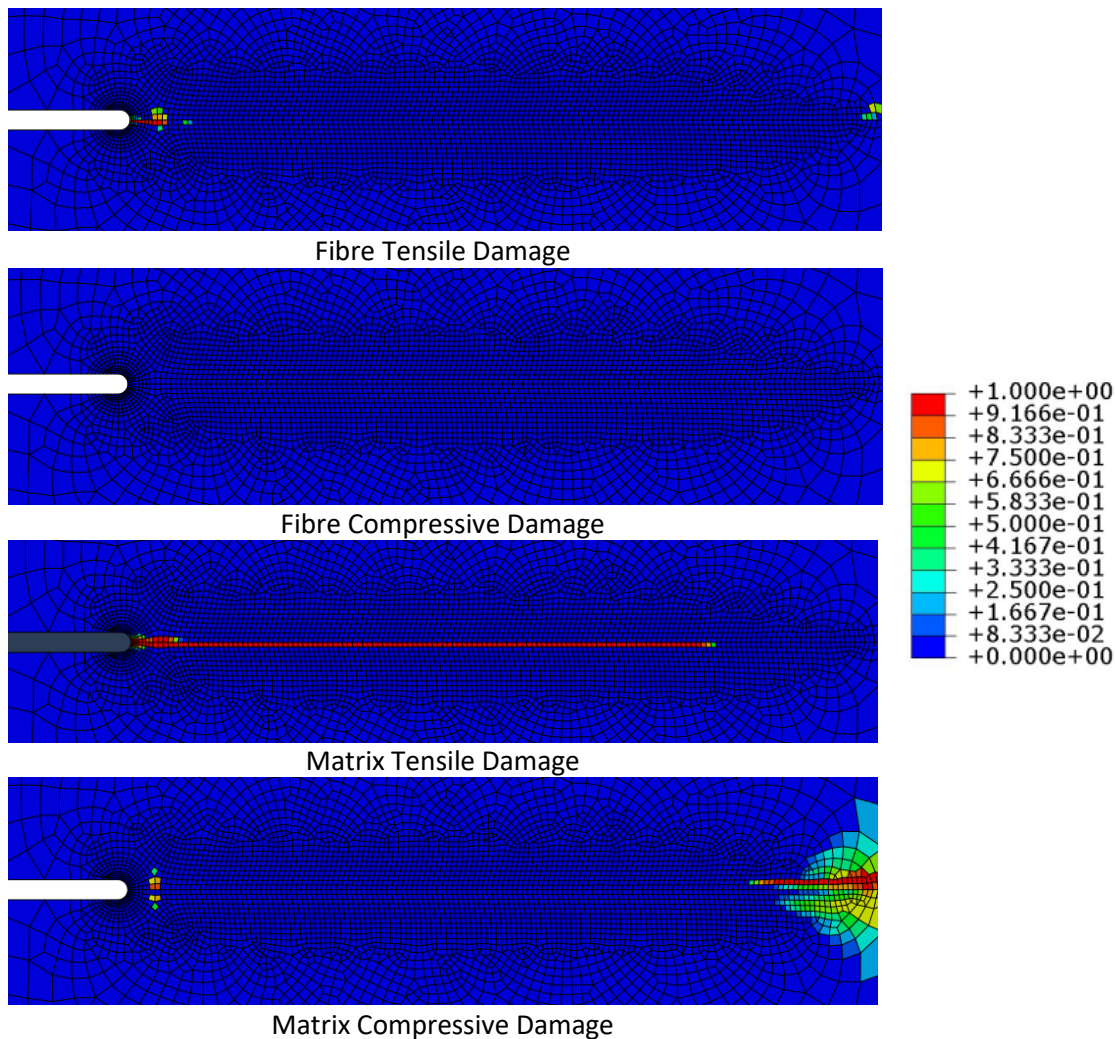


Figure 8 – Final damage distribution for the Hashin failure model.

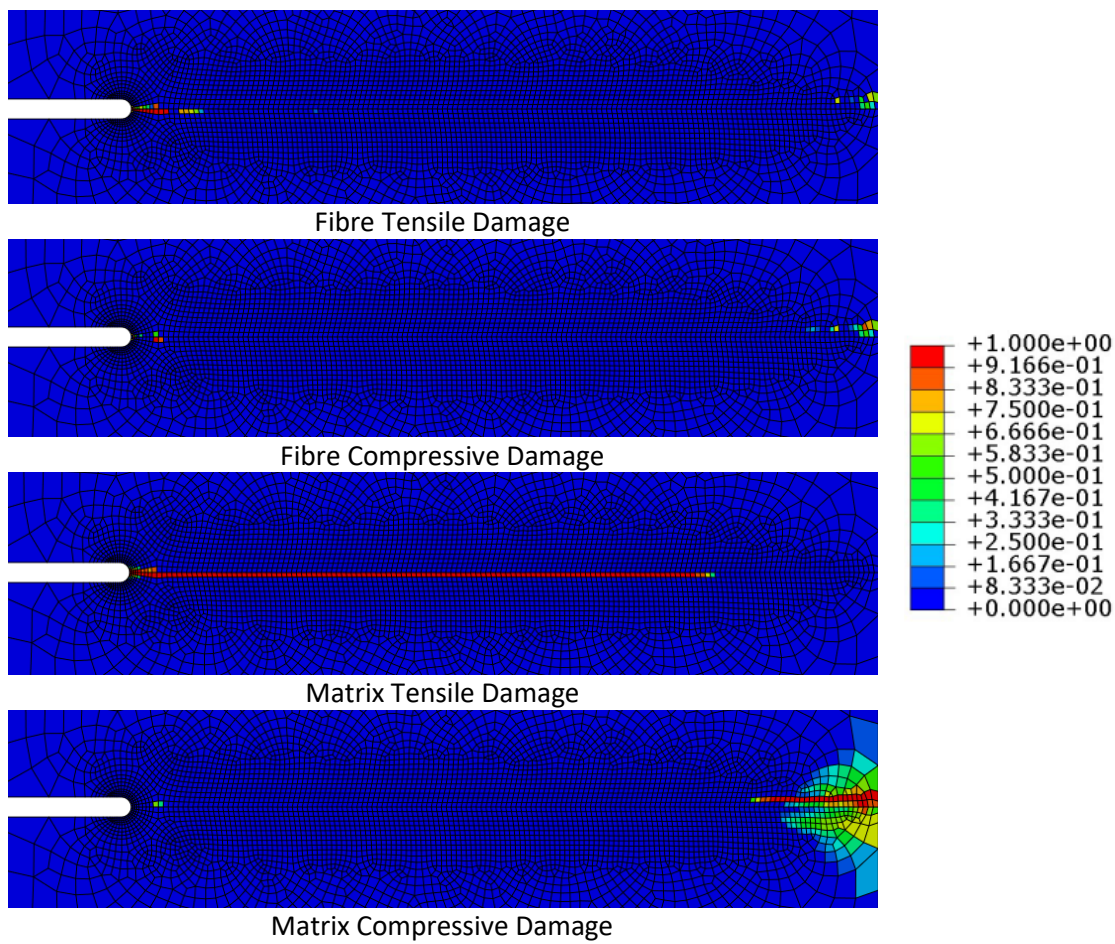


Figure 9 – Final damage distribution for the Tsai-Wu failure model with MDE.

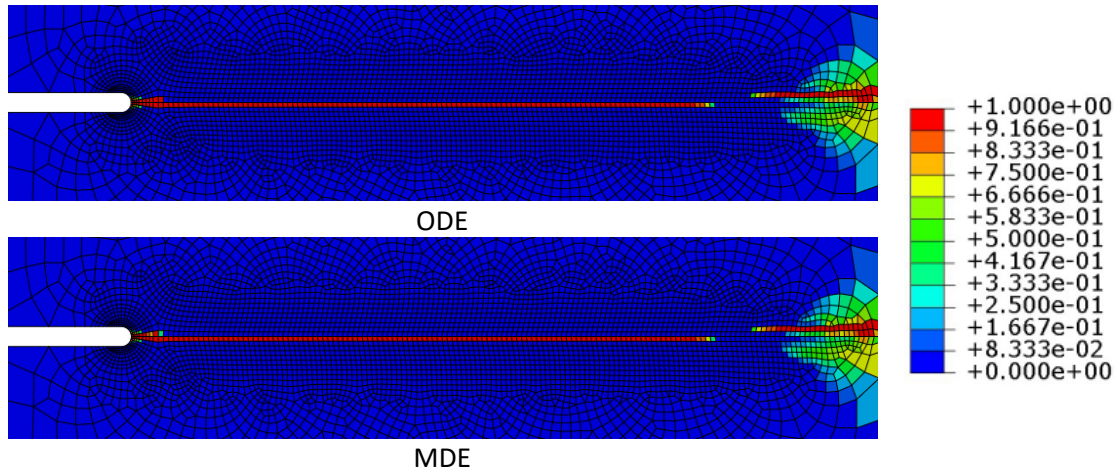


Figure 10 – Final shear damage distribution for the Tsai-Wu failure model with ODE and MDE.

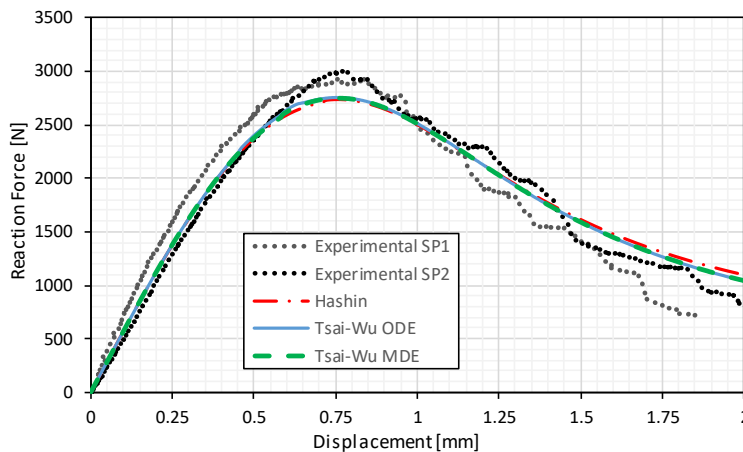


Figure 11 – Force vs. vertical displacement response in the master joint for the CT tests.

4.2 Pultruded GFRP Beam with Three-Point Bending

The purpose of this example – pultruded GFRP beam in three-point bending with a notch at midspan – originally presented by [34], was to experimentally assess the mode I fracture properties of pultruded GFRP composites along the fibre direction. The original authors [34] have used a bilinear softening constitutive law in order to determine the fracture energy. In the present work, an exponential softening constitutive law is used in this test, which is the one chosen in the work of [11, 12]. The properties adopted for this numerical model are the ones provided in [34]. In any case, because some properties were not provided in that reference, data corresponding to similar pultruded GFRP materials available in the literature were adopted from section 3.1 and are listed in **Table 2**.

Table 2 – Properties for GFRP material of the beam (* are the ones adopted).

E_1 [MPa]	E_2 [MPa]	G_{12} [MPa]	ν_{12} [-]	$X_t = X_c$ [MPa]
15000*	10800	2000*	0.24*	323*
Y_t/Y_c [MPa]	S_L [MPa]	S_T [MPa]	$G_{ft} = G_{fc}$ [MPa.mm]	$G_{mt} = G_{mc}$ [MPa.mm]
37/80*	33	33	100*	7.8

To reduce the computational cost, a symmetry simplification is adopted, and only half of the beam is analysed, as shown in **Figure 12 a)**. The notch is 2 mm wide and 15 mm deep, corresponding to a specimen height ratio of 0.3.

Different mesh refinement strategies are considered in two regions of the beam. As shown in **Figure 12 b)**, in the neighbourhood of the right notch a very refined mesh is adopted, with a maximum element size of 0.25 mm. The meshes in both parts are linked using a tie constraint in order to enforce the correct kinematic conditions between unlinked nodes.

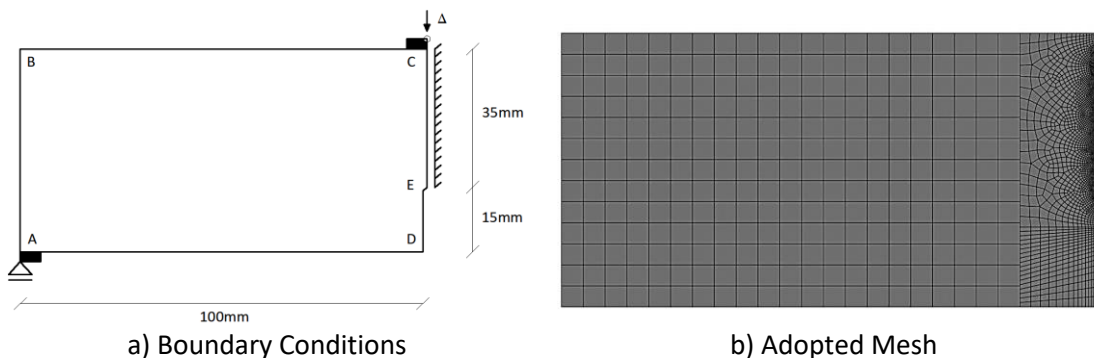


Figure 12 – Boundary conditions and adopted mesh for the specimen with thickness of 18mm.

Figure 13 plots the force vs. vertical displacement curves obtained from the experiments and the numerical simulations. It can be seen that none of the damage models being tested are able to correctly simulate the elastic stiffness. This may be explained by the fact that local crushing may have occurred near the support, and that effect was not simulated by the numerical models. In any case, the maximum force provided by the numerical model lies between the experimental upper and lower bounds. It is also important to point out that the softening branches recovered of both failure models (Hashin and Tsai-Wu) present some differences when compared to the ones observed in the experiments. In fact, the softening branch of the experimental curves presents a higher slope. This difference may be associated to some inaccuracies in the definition of the damage model parameter values (as mentioned, some of which had to be assumed). When the Tsai-Wu failure model is used, both alternative ODE and MDE variants present very similar responses.

Figure 14 displays the final damage distribution near the notch for the Hashin and the MDE Tsai-Wu failure models. It is possible to conclude that both models present the same tensile and compressive damage distribution. A very small difference exists in the compressive matrix damage, near the top support, mainly due to the concentrated load.

Figure 15 a) plots the maximum principal stress vs. maximum principal strain diagram, computed at the top of the notch. In this case both models present a good agreement, thus confirming that the state directional variable is correctly simulating the damage evolution. The same conclusion can be drawn from the analysis of **Figure 15 b**, in which the matrix damage value is plotted as a function of the principal strain, also at the top of the notch.

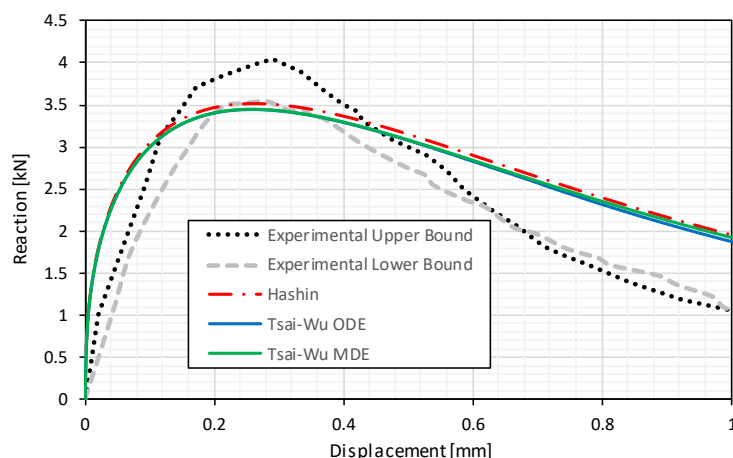


Figure 13 – Force vs. vertical displacement response of the GFRP beam: experimental and numerical results.

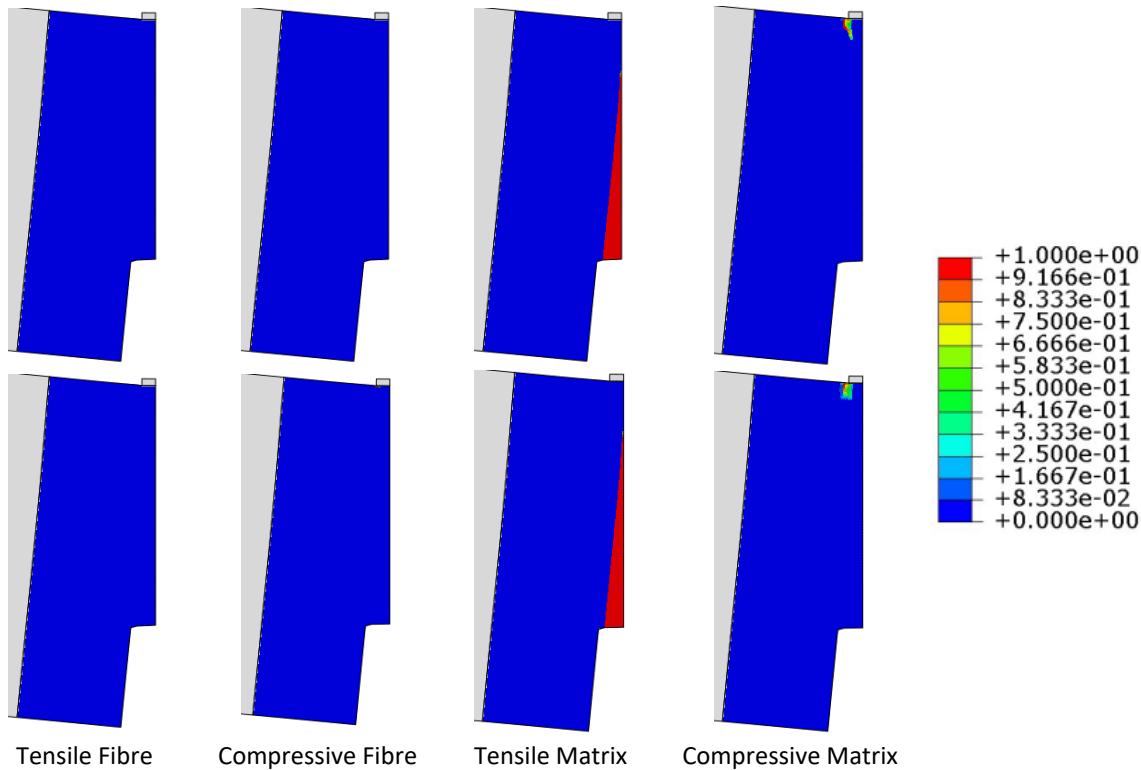


Figure 14 – Final damage distribution, on the top for the Hashin failure model, and on the bottom for the Tsai-Wu damage model with MDE.

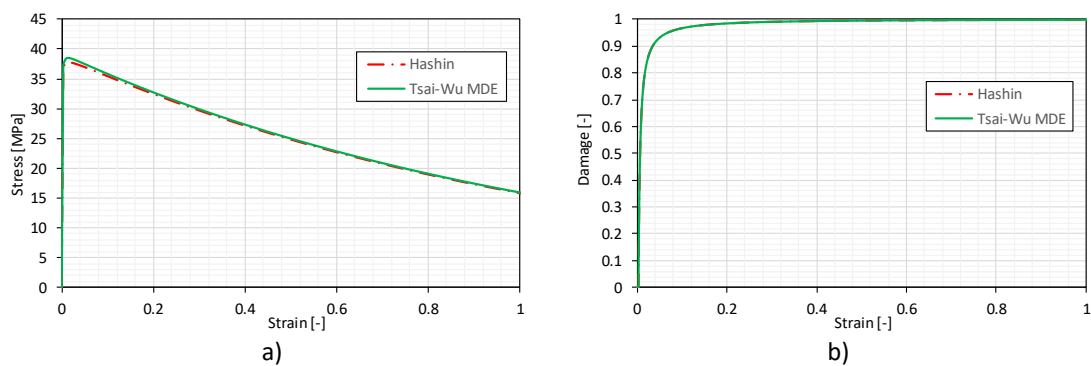


Figure 15 – a) Principal maximum stress vs. strain; b) matrix damage evolution for the Hashin and Tsai-Wu (MDE) failure models.

4.3 Double-Lap Bolted Connection with Shear Out Failure

This example was recently presented by Viet *et al.* in [35], who conducted an extensive experimental campaign on several bolted double lap connections between GFRP laminates, in which properties, geometries, shear out and bearing collapse mechanisms were reported. According to recent findings [36], the use of a linear softening constitutive law provides good results, allowing to simulate shear-out and bearing failure, if a residual shear stress is considered in the constitutive law. Therefore, for this example, a linear softening constitutive law with residual stress is used. Even if there is still no consensus in the scientific community regarding

the value to be adopted for the residual stress, a value corresponding to 15% of the compressive strength is adopted here according to recent findings reported in [12]. It is important to point out that this residual stress is required to better simulate the compressive behavior associated to crushing.

The equivalent properties adopted for this model are in part provided by the original authors in [35]. For the properties not provided there, values available in the literature for similar materials are considered. This is necessary in an homogenized laminate, since the specimen is assembled from different materials, which cannot be correctly simulated throughout the laminate thickness, with a simple plane stress analysis.

Table 3 – Properties of the GFRP in the shear out specimen (* are the ones adopted).

$E_1 [MPa]$	$E_2 [MPa]$	$G_{12} [MPa]$	$\nu_{12} [-]$	$X_t = X_c [MPa]$
23000*	12000*	3000*	0.24*	323*
$Y_t = Y_c [MPa]$	$S_L [MPa]$	$S_T [MPa]$	$G_{ft} = G_{fc} [MPa.mm]$	$G_{mt} = G_{mc} [MPa.mm]$
27	27	22	100*	20*

The boundary conditions around the hole are identical to the ones defined in the first example, with some slight differences due to the symmetry simplifications being adopted, as depicted in **Figure 16**. The mesh was refined near the zones where shear damage may occur.

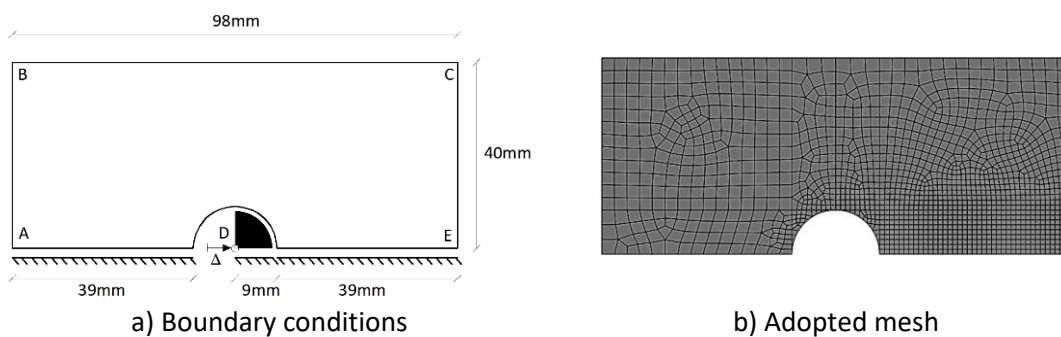


Figure 16 – Boundary conditions and adopted mesh for the double-lap bolted connection with shear-out failure, with equivalent thickness of 6.5 mm.

Figure 17 presents the load vs. displacement curves, obtained from the experimental tests and the numerical simulations, considering both damage models. For the experimental campaign, only the upper and lower bound curves are presented. Taking into account that in the experimental data, due to the initial flexibility of the connection for low load levels, the displacements in these curves were adjusted. It is possible to verify that the experimental elastic response is more flexible than the one obtained with the numerical models. This is expected, as the real model is always less stiff due to non-rigid contact and some crushing that may occur in the bolt (in the bolt hole contour), which is not simulated in the numerical models.

The results presented in **Figure 17** show that the Tsai-Wu failure model with ODE is clearly unable to correctly simulate the shear-out collapse. This happens because in this model the shear damage evolves fast and with a “brittle” behaviour, due to the quadratic shear damage growth defined by equation (18). This is not the case when the Hashin failure model is used, in which the tensile and compressive damage never occur simultaneously. To minimize this drawback, the authors propose the use of the MDE technique. In any case, even when using the MDE model, a premature force drop still occurs after the maximum force is reached. That effect

does not occur neither in the experiments nor in the numerical simulations based on the use of the Hashin failure model. This suggests that the MDE is also not able to completely and accurately simulate shear damage, and this is an issue that has to be addressed in the near future, by developing a consistent damage model with shear energy.

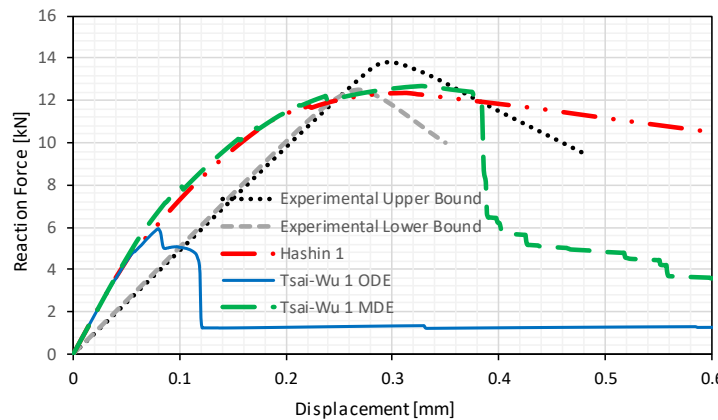
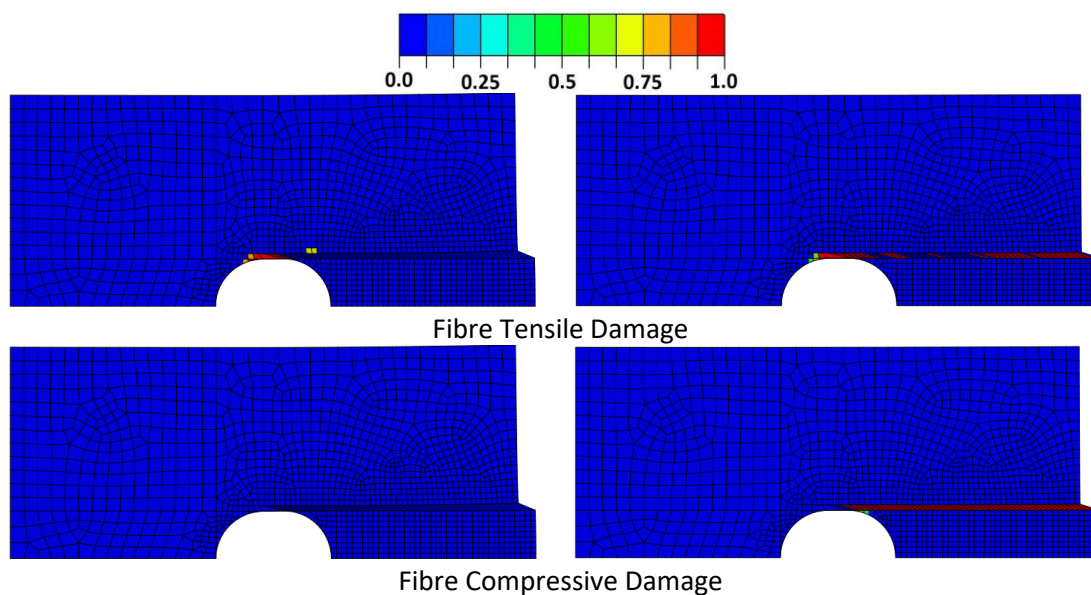


Figure 17 – Force vs. horizontal displacement response for the double-lap bolted connection with shear-out failure.

Figure 18 shows the final damage distribution together with the laminate deformed shape for both Hashin and Tsai-Wu MDE failure models. The main difference corresponds to the tensile and compressive damage values that are obtained, which are more severe in the case of the Tsai-Wu failure model, because all damage modes are activated at the same time. In any case, the damage evolution is controlled by the directional state variable, defined by equations (38) and (39), in order to prevent unrealistic damage growth. Some other slight differences in the matrix damage distribution may be observed. Near collapse, the shear damage distribution provided by both damage models is quite similar.



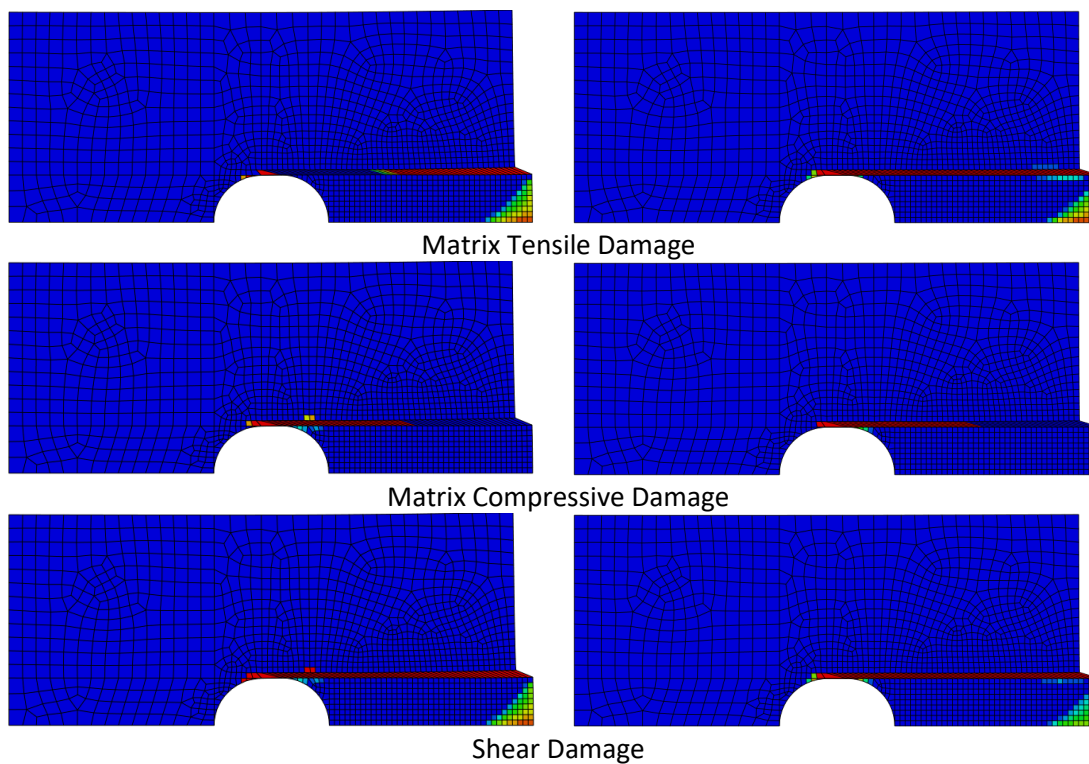
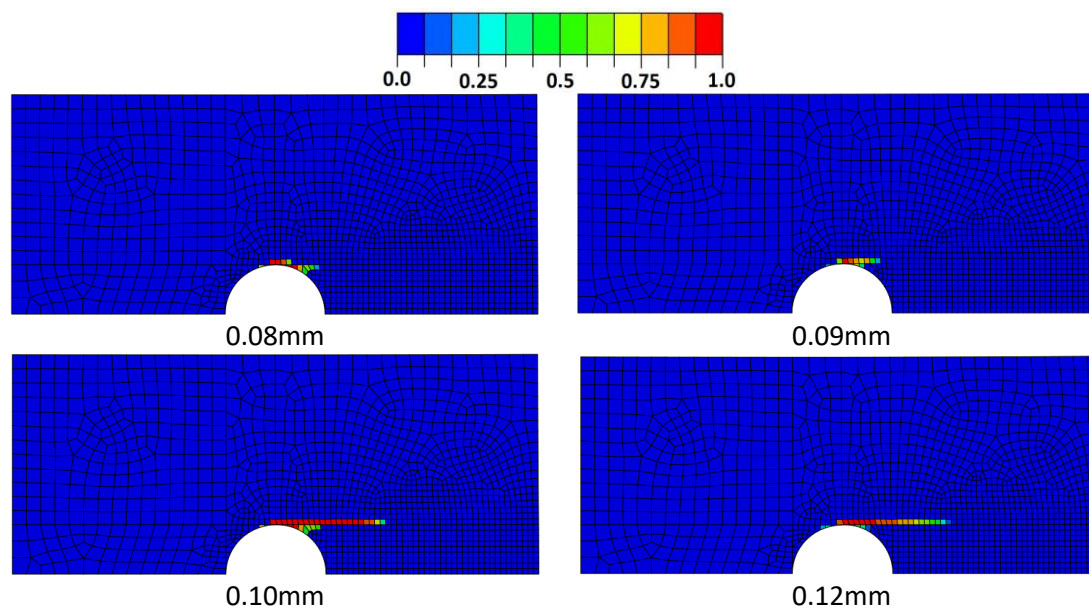


Figure 18 – Final damage distribution, on the left for the Hashin failure model, and on the right for the Tsai-Wu failure model with MDE.

Figure 19 presents the shear damage evolution obtained with both the Tsai-Wu ODE and MDE damage models. Even if the final shear damage distribution is similar, the final shear-out mechanism occurs for a much larger prescribed displacement value when the MDE algorithm is considered. This mechanism occurs for a displacement of around 0.4 mm, almost four times greater than the one observed when the ODE damage model is considered.



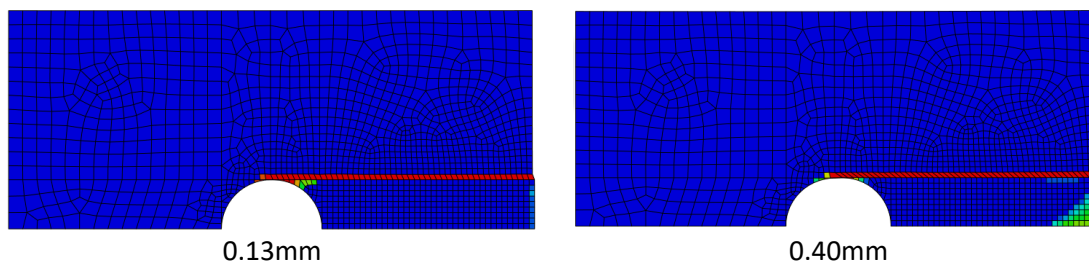
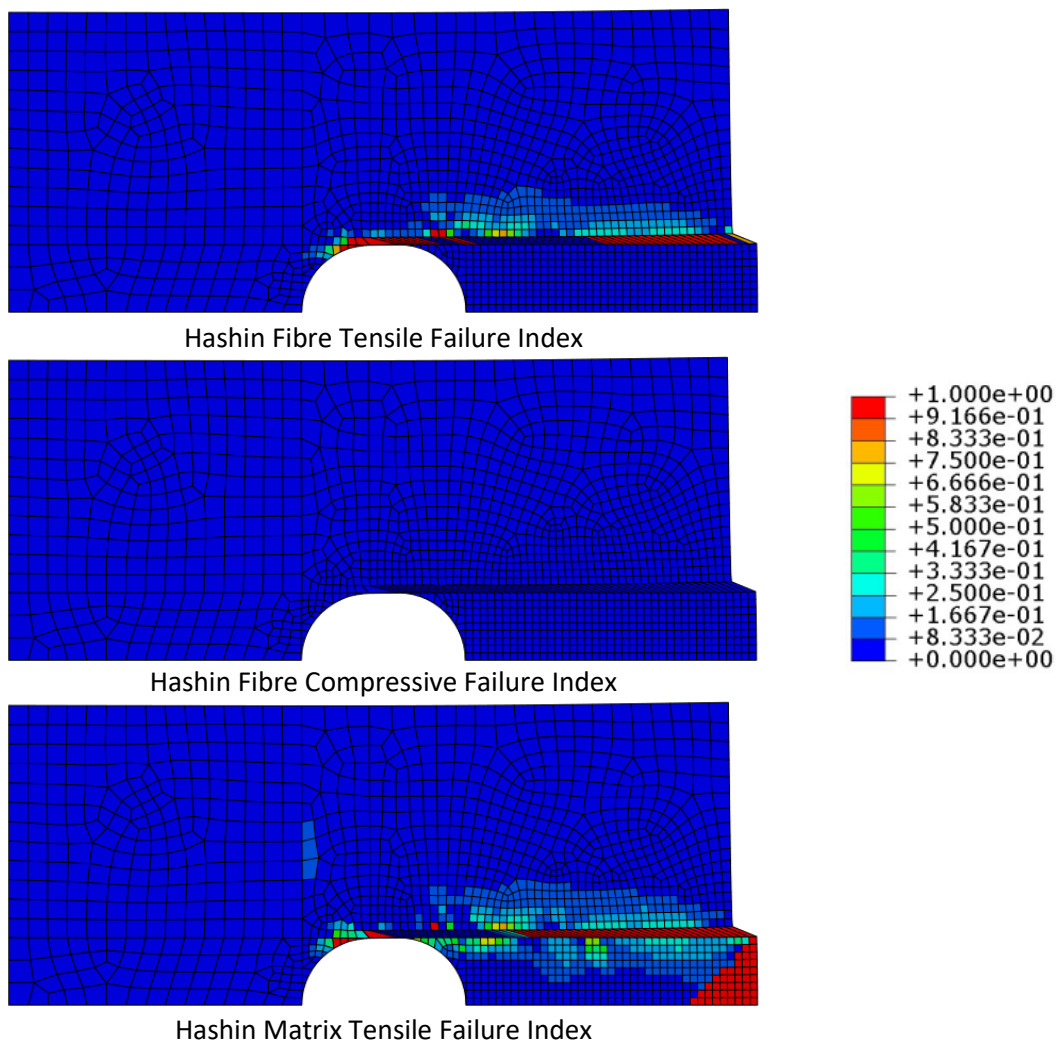


Figure 19 – Shear damage evolution for the Tsai-Wu failure model, with ODE on the left and MDE in the right, for increasing values of the prescribed displacement.

The difference between the failure indexes (3) obtained with the Hashin and Tsai-Wu MDE models are represented in **Figure 20**. The differences illustrated in this figure, concerning damage evolution, were already expected, since in the Tsai-Wu failure model the failure criterion is a single quadratic function, while the Hashin model comprises four separate functions. **Figure 20** shows that the final damage distribution is very different even if the final shear damage distribution is quite similar. This again is explained by the state directional variable controlling the damage evolution when the Tsai-Wu failure index reaches the value of 1. This is the main reason why the structural response is quite similar in both models.



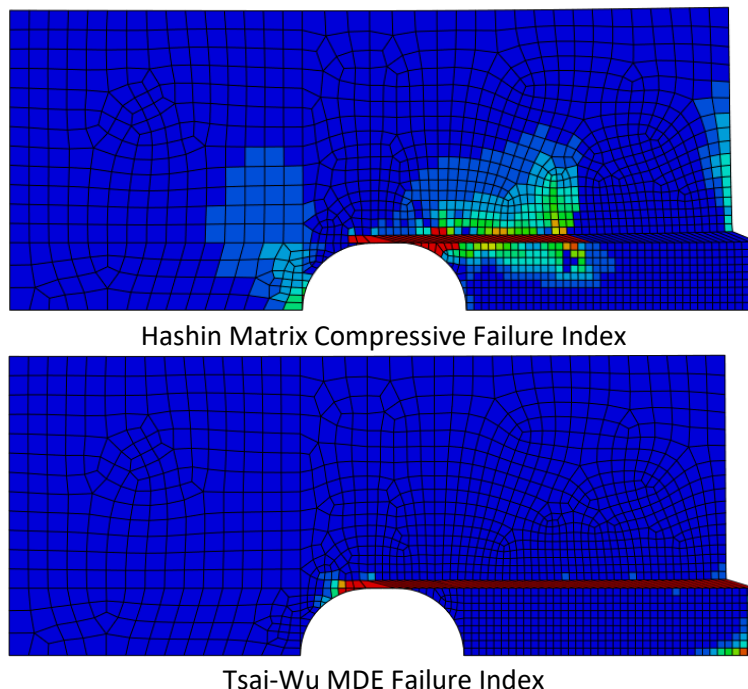


Figure 20 – Final distributions of the failure index for the Hashin and Tsai-Wu MDE failure models.

Figure 21 shows a diagram with the average shear stress (tangent to the hole, the direction of the shear damage propagation) vs. shear strain, for the Hashin and Tsai-Wu MDE and ODE failure models. It is important to point out that this shear stress is always combined with other stresses, when computing the equivalent stresses and strains. Therefore, some differences may exist between the results provided by different damage models, depending on the constitutive damage evolution. **Figure 21** shows that the Tsai-Wu ODE model provides a slightly lower maximum shear stress when compared with the Hashin failure model, but the softening regime of the former model is much more brittle. On the other hand, the Tsai-Wu MDE model provides an apparent higher shear resistance (38%), but the post-peak damage evolution is quite consistent with that of the Hashin failure model. It is important to point out that for the three damage models being tested, the resistance values provided in **Table 3** are never exceeded.

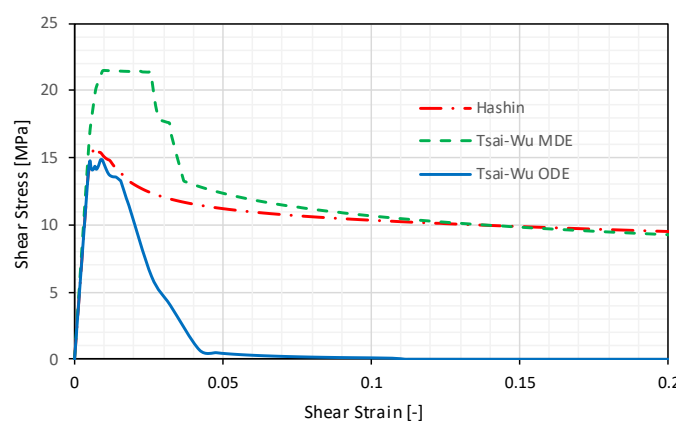


Figure 21 – Shear stress vs. shear strain tangent to the hole for the Hashin and Tsai-Wu MDE and ODE failure models.

5 Conclusions and Further Developments

In this work a new 2D orthotropic damage model based on the Tsai-Wu failure criterion is proposed and tested, implemented through a user-defined material (UMAT) subroutine of the commercial finite element software ABAQUS. The main focus was to demonstrate that it is possible to assemble an orthotropic damage model, with a single failure criterion, just like in isotropic materials. Several examples were tested, in which experimental data available in the literature was compared to the numerical results obtained with the proposed model, and also with the classical Hashin-based orthotropic failure model considered as reference. The results obtained and discussed in this study allow drawing the following conclusions:

- 1) In general, the proposed Tsai-Wu failure model presented good results when compared with the popular Hashin failure model, provided that the modified damage evolution (MDE) law is used. On the other hand, the use of the original damage evolution (ODE) with the proposed Tsai-Wu failure model did not provide accurate results when there is a great influence of shear damage, particularly in the simulation of shear-out collapse.
- 2) When using the Tsai-Wu failure model, the shear damage associated to the ODE is clearly more brittle than the one obtained with the MDE variant. Besides, the maximum shear stress in the ODE variant tends to be slightly lower when compared to the one provided by the Hashin failure model.
- 3) Overall, for the three examples presented in this work, the proposed Tsai-Wu failure model was able to provide a good agreement with experimental results. Some of the reported differences may be attributed to some unknown material properties (not provided in the original references), which had to be assumed in the present study.
- 4) The Tsai-Wu failure index evolves differently from the ones provided by the classical Hashin failure model, especially when there is significant shear damage. In any case, when comparing the fibre and matrix damage evolution and the stress vs. strain curves, both models present a good agreement. This is due to the consideration of the state direction variable, that contributes to correct the damage evolution, when the Tsai-Wu failure criterion is reached.
- 5) As in the Tsai-Wu failure model all damage variables evolve simultaneously, in all examples presented in this work, the forces after softening are slightly lower than the ones computed using the classical Hashin failure model.

Future research will focus on the development of the damage based Tsai-Wu failure model for cyclic loads by introducing permanent strains and hysteretic loops in the formulation. This is important to study the energy dissipation in GFRP composite structures under cyclic loading (e.g. earthquakes). This is a major gap in existing literature. Also planned is the upscale of this formulation to 3D analysis, which will be mainly applied to study beam-to-column GFRP connections. Another effort will be made to improve the shear damage evolution for the case of the MDE law, by using mixed shear modes in the global response, something already attempted by other authors with the various damage models [1].

Acknowledgements

This work has been partly supported by Fundação para a Ciência e Tecnologia (FCT), under the Transitional Standard – DL57/2016/N3/UI/CERIS/CT/165/2018, and under the PhD scholarship SFRH/BD/109957/2015.

References

- [1] Barbero EJ. Finite Element Analysis of Composite Materials using ABAQUS. London: CRC Press, 2013.
- [2] Pinho S, Vyas G, Robinson P. Material and structural response of polymer-matrix fibre-reinforced composites: Part B. *Journal of Composite Materials*. 2013;47(6-7):679-96 DOI: 10.1177/0021998313476523.
- [3] Osswald PV, Osswald TA. A strength tensor based failure criterion with stress interactions. *Polymer Composites*. 2018;39(8):2826-34 DOI: <https://doi.org/10.1002/pc.24275>.
- [4] Camanho PP, Arteiro A, Melro AR, Catalanotti G, Vogler M. Three-dimensional invariant-based failure criteria for fibre-reinforced composites. *International Journal of Solids and Structures*. 2015;55:92-107 DOI: <https://doi.org/10.1016/j.ijsolstr.2014.03.038>.
- [5] Zappino E, Filippi M, Pagani A, Petiti M, Carrera E. Experimental and numerical analysis of 3D printed open-hole plates reinforced with carbon fibers. *Composites Part C: Open Access*. 2020;2:100007 DOI: <https://doi.org/10.1016/j.jcomc.2020.100007>.
- [6] Gol'denblat II, Kopnov VA. Strength of glass-reinforced plastics in the complex stress state. *Polymer Mechanics*. 1965;1(2):54-9 DOI: 10.1007/BF00860685.
- [7] Hashin Z. Failure Criteria for Unidirectional Fiber Composites. *Journal of Applied Mechanics*. 1980;47(2):329-34 DOI: 10.1115/1.3153664.
- [8] Lapczyk I, Hurtado JA. Progressive damage modeling in fiber-reinforced materials. *Composites Part A: Applied Science and Manufacturing*. 2007;38(11):2333-41 DOI: <https://doi.org/10.1016/j.compositesa.2007.01.017>.
- [9] Camanho PP, Catalanotti G. On the relation between the mode I fracture toughness of a composite laminate and that of a 0° ply: Analytical model and experimental validation. *Engineering Fracture Mechanics*. 2011;78(13):2535-46.
- [10] Li S, Sitnikova E, Liang Y, Kaddour A-S. The Tsai-Wu failure criterion rationalised in the context of UD composites. *Composites Part A: Applied Science and Manufacturing*. 2017;102:207-17 DOI: <https://doi.org/10.1016/j.compositesa.2017.08.007>.
- [11] Almeida-Fernandes L, Silvestre N, Correia JR, Arruda MRT. Fracture toughness-based models for damage simulation of pultruded GFRP materials. *Composites Part B: Engineering*. 2020;186:107818 DOI: <https://doi.org/10.1016/j.compositesb.2020.107818>.
- [12] Almeida-Fernandes L, Silvestre N, Correia JR, Arruda M. Compressive transverse fracture behaviour of pultruded GFRP materials: Experimental study and numerical calibration. *Composite Structures*. 2020;247:112453 DOI: <https://doi.org/10.1016/j.compstruct.2020.112453>.
- [13] Lemaitre J, Chaboche JL. Mécanique des matériaux solides: Dunod, 1985.
- [14] Tsai SW, Wu EM. A General Theory of Strength for Anisotropic Materials. *Journal of Composite Materials*. 1971;5(1):58-80 DOI: 10.1177/002199837100500106.
- [15] Kaddour A, Hinton M. Maturity of 3D failure criteria for fibre-reinforced composites: Comparison between theories and experiments: Part B of WWFE-II. *Journal of Composite Materials*. 2013;47(6-7):925-66 DOI: 10.1177/0021998313478710.
- [16] Tsai SW. A Survey of Macroscopic Failure Criteria for Composite Materials. *Journal of Reinforced Plastics and Composites*. 1984;3(1):40-62 DOI: 10.1177/073168448400300102.
- [17] Tsai SW, Hahn HT. Introduction to composite materials. Westport, Conn.: Technomic Pub., 1980.

- [18] Proença SPB. Introdução à mecânica do dano e fracturamento, Notas de aulas. Escola de Engenharia de São Carlos, Universidade de São Carlos, São Paulo 2000.
- [19] Ziegler H. An introduction to thermomechanics. North-Holland 1977.
- [20] Lemaitre J, Benallal A, Billardon R, Marquis D. Thermodynamics and phenomenology. In Continuum Thermomechanics - The Art and Science of Modelling Material Behaviour, Solid Mechanics and Its Applications. 2002;76:209-23 Springer Netherlands.
- [21] Nguyen QS. Uniqueness, stability and bifurcation of standard systems. Current Trends and Results in Plasticity. London: Elsevier; 1985.
- [22] Matzenmiller A, Lubliner J, Taylor RL. A constitutive model for anisotropic damage in fiber-composites. Mechanics of Materials. 1995;20(2):125-52 DOI: [http://dx.doi.org/10.1016/0167-6636\(94\)00053-0](http://dx.doi.org/10.1016/0167-6636(94)00053-0).
- [23] Lemaitre J, Desmorat R. Engineering Damage Mechanics. Berlin Heidelberg: Springer, 2005.
- [24] ABAQUS. Abaqus Unified FEA. Rhode Island: SIMULIA.
- [25] Bazant ZP, Oh BH. Crack band theory for fracture of concrete. Materials and Structures. 1983;16:155-77.
- [26] Wang C, Roy A, Silberschmidt VV, Chen Z. Modelling of Damage Evolution in Braided Composites: Recent Developments. Mechanics of Advanced Materials and Modern Processes. 2017;3(1):15 DOI: 10.1186/s40759-017-0030-4.
- [27] Borst R, Crisfield MA, Remmers JJC, Verhoosel CV. Nonlinear Finite Element Analysis of Solids and Structures. UK: Wiley, 2012.
- [28] Duvaut G, Lions JL. Les Inéquations en Mécanique et en Physique. Paris: Dunod, 1972.
- [29] Geers MGD, Brekelmans WAM, de Borst R. Viscous Regularization of Strain-Localisation for Damaging Materials. Dordrecht: Springer Netherlands; 1994. p. 127-38.
- [30] Dunne F, Petrinic N. Introduction to Computational Plasticity. New York: Oxford University Press, 2005.
- [31] Lopes B, Arruda MRT, Almeida-Fernandes L, Castro L, Silvestre N, Correia JR. Assessment of mesh dependency in the numerical simulation of compact tension tests for orthotropic materials. Composites Part C: Open Access. 2020;1:100006 DOI: <https://doi.org/10.1016/j.jcomc.2020.100006>.
- [32] Almeida-Fernandes L, Silvestre N, Correia JR. Characterization of transverse fracture properties of pultruded GFRP material in tension. Composites part B Engineering. 2019;175(15) DOI: doi.org/10.1016/j.compositesb.2019.107095.
- [33] Girão Coelho AM, Toby Mottram J, Harries KA. Finite element guidelines for simulation of fibre-tension dominated failures in composite materials validated by case studies. Composite Structures. 2015;126:299-313 DOI: <https://doi.org/10.1016/j.compstruct.2015.02.071>.
- [34] Liu W, Feng P, Huang J. Bilinear softening model and double K fracture criterion for quasi-brittle fracture of pultruded FRP composites. Composite Structures. 2017;160:1119-25 DOI: <https://doi.org/10.1016/j.compstruct.2016.10.134>.
- [35] Phan Viet N, Satria Yoresta F, Kitane Y, Hashimoto K, Matsumoto Y. Improving the shear strength of bolted connections in pultruded GFRP using glass fiber sheets. Composite Structures. 2021;255:112896 DOI: <https://doi.org/10.1016/j.compstruct.2020.112896>.
- [36] Zhuang F, Arteiro A, Furtado C, Chen P, Camanho PP. Mesoscale modelling of damage in single- and double-shear composite bolted joints. Composite Structures. 2019;226:111210 DOI: <https://doi.org/10.1016/j.compstruct.2019.111210>.